# Multitracer technique for galaxy bispectrum: An application to constraints on nonlocal primordial non-Gaussianities

Daisuke Yamauchi,[1,*] Shuichiro Yokoyama,[2] and Keitaro Takahashi[3]
[1]*Faculty of Engineering, Kanagawa University, Kanagawa 221-8686, Japan*
[2]*Department of Physics, Rikkyo University, Tokyo 171-8501, Japan*
[3]*Faculty of Science, Kumamoto University, 2-39-1 Kurokami, Kumamoto 860-8555, Japan*
(Received 23 November 2016; published 30 March 2017)

We explore the use of galaxy bispectra with the multitracer technique as a possible probe of primordial non-Gaussianities. We forecast future constraints on non-linearity parameters, $f_{\rm NL}^{\rm eq}$ and $f_{\rm NL}^{\rm orth}$, which, respectively, characterize the equilateral- and orthogonal-type primordial bispectra, and show that the multitracer analysis would be effective with reducing the cosmic-variance noise if the number density of galaxies is high enough. We find that the measurement of the galaxy bispectrum by future galaxy surveys can reach the constraints on the nonlocal-type primordial non-Gaussianities to the level more severe than current one which has been obtained by cosmic microwave background observations.

DOI: 10.1103/PhysRevD.95.063530

## I. INTRODUCTION

Primordial non-Gaussianity (PNG), recently, has been expected to be one of the most informative fingerprints of inflation and brings insights into the fundamental physics behind inflation. Since different shapes of higher-order primordial spectra can be linked to a different mechanism for generating non-Gaussian features of the primordial fluctuations, it would be interesting to constrain various types of PNG by precise cosmological measurements such as the cosmic microwave background (CMB) and large-scale structure (LSS).

The amplitudes in the various shapes of the primordial bispectrum are basically characterized by three so-called non-linearity parameters $f_{\rm NL}^{\rm local}$, $f_{\rm NL}^{\rm eq}$, and $f_{\rm NL}^{\rm orth}$, which, respectively, correspond to the amplitudes of the *local* [1], *equilateral* [2], and *orthogonal* types [2]. These are frequently considered as typical examples and are strongly motivated by inflationary models. The current limits on these parameters have been obtained from the CMB temperature anisotropies and polarizations: $f_{\rm NL}^{\rm local} = 0.8 \pm 5.0$, $f_{\rm NL}^{\rm eq} = -4 \pm 43$, and $f_{\rm NL}^{\rm orth} = -26 \pm 21$ at $1\sigma$ statistical significance, respectively [3,4]. Although such strict constraints on the non-linearity parameters have not been obtained from the observational data of the LSS yet, the spatial clustering behavior of the halos/galaxies on large scales is believed to be a powerful tool to probe the PNG. One of the most distinctive effects of the PNG on the clustering of the galaxies is known as the *scale-dependent bias* (see, e.g., Refs. [5,6]), which is due to the non-linear coupling caused by PNG, and it is expected to have a potential to reach $\sigma(f_{\rm NL}^{\rm local}) = \mathcal{O}(0.1\text{–}1)$ in future surveys.

It is, however, shown that the scale-dependent clustering property due to PNG extracted from the galaxy power spectrum is too weak to detect except for the local type, implying that the scale-dependent clustering is irrelevant for the nonlocal type PNG [7]. Then, the bispectrum of the biased objects such as the halo/galaxy has been considered as one of the useful observables to obtain constraints on the nonlocal-type PNG. Although the halo/galaxy bispectrum should be generated from the late-time non-linear gravitational evolution of the density fluctuations, the contribution from the nonlocal-type PNG would be dominant on larger scales (see, e.g., Refs. [8–12]). We then expect that the property of the scale dependence of the galaxy bispectrum provides us the opportunity to probe not only the local- but also nonlocal-type PNG with precise measurements of the LSS in future. However, the clustering analysis at large scales is limited due to cosmic variance (CV), because of the lack of enough independent measurements. A possible way to reduce the CV noise is the use of the multitracer technique [13,14], in which the availability of multiple tracers with different biases allows significant improvements in the statistical errors. The clustering analysis with the multitracer technique has been previously studied only in the case of the power spectrum for future galaxy surveys such as Euclid[1] and SKA,[2] and the effect turns out to be indeed very effective, and we can reach $\sigma(f_{\rm NL}^{\rm local}) = \mathcal{O}(1)$ [15–20] even when the horizon-scale effects are taken into account [21–24]. However, the multitracer method for the higher moments has not been discussed in the literature.

In this paper, thus, we consider the galaxy bispectrum as the probe of the various types of PNG and derive the formulas for the monopole mode of the bispectrum from

*yamauchi@jindai.jp

[1]See http://www.euclid-ec.org.
[2]See http://www.skatelescope.org.

 

the redshift-space distortion (RSD) generalized to multiple tracers to apply the multitracer method. Based on the derived analysis tool, we then calculate the expected galaxy bispectrum, and the possibility to detect the PNG is discussed.

## II. BISPECTRUM WITH MULTIPLE TRACERS

The power spectrum, $P^{(g_1g_2)}(k)$, and bispectrum, $B^{(g_1g_2g_3)}(k_1,k_2,k_3)$, where we have used an index $g_i$ as a label of the tracer objects such as galaxies, can be defined in terms of the Fourier components of the number density field of the tracer objects, $\delta^{(g_i)}(\boldsymbol{k})$, as

$$\langle\delta^{(g_1)}(\boldsymbol{k})\delta^{(g_2)}(\boldsymbol{k}')\rangle = (2\pi)^3\delta_{\rm D}^3(\boldsymbol{k}+\boldsymbol{k}')P^{(g_1g_2)}(k), \quad (1)$$

$$\langle\delta^{(g_1)}(\boldsymbol{k}_1)\delta^{(g_2)}(\boldsymbol{k}_2)\delta^{(g_3)}(\boldsymbol{k}_3)\rangle = (2\pi)^3\delta_{\rm D}^3(\boldsymbol{k}_1+\boldsymbol{k}_2+\boldsymbol{k}_3)B^{(g_1g_2g_3)}(k_1,k_2,k_3), \quad (2)$$

where $\delta_{\rm D}^3$ is a three-dimensional Dirac delta function. Even if the initial condition for density fluctuations is assumed to be Gaussian, the non-linear gravitational evolution naturally induces the non-negligible non-Gaussianity. In the large-scale limit where the scale of interest is much larger than the typical scale of the collapsed objects, the bispectrum of the tracer objects can be decomposed into several parts [9]. Hereafter, we focus on the dominant contributions on large scales, and let us consider the contributions from the gravitational evolution and the primordial bispectrum, $B_{\rm grav}$ and $B_{\rm bis}$, which can be simply written as [8,9]

$$B_{\rm grav}^{(g_1g_2g_3)} = \frac{1}{6}[b_1^{(g_1)}b_1^{(g_2)}(b_2^{(g_3)}+2b_1^{(g_3)}F_2(\boldsymbol{k}_1,\boldsymbol{k}_2)) + (g_i\text{perm})]P_{\rm L}(k_1)P_{\rm L}(k_2) + (k_i\text{perm}), \quad (3)$$

$$B_{\rm bis}^{(g_1g_2g_3)} = b_1^{(g_1)}b_1^{(g_2)}b_1^{(g_3)}B_{\rm L}(k_1,k_2,k_3), \quad (4)$$

where $P_{\rm L}(k)$ and $B_{\rm L}(k_1,k_2,k_3)$ are, respectively, a power spectrum and a bispectrum for the linear density field, $\delta_{\rm L}$. The linear density field can be related to the primordial curvature perturbations $\Phi$ through the Poisson equation as $\delta_{\rm L}(\boldsymbol{k},z) = \mathcal{M}(k;z)\Phi(\boldsymbol{k})$ with $\mathcal{M}(k;z) = 2D_+(z)k^2T(k)/3H_0^2\Omega_{\rm m,0}$, where $D_+(z)$ and $T(k)$ represent the linear growth rate and matter transfer function normalized to unity at the large scale [25], respectively. Based on this expression, we can rewrite $P_{\rm L}$ and $B_{\rm L}$ as $P_{\rm L}(k) = \mathcal{M}^2(k)P_\Phi(k)$ and $B_{\rm L}(k_1,k_2,k_3) = \mathcal{M}(k_1)\mathcal{M}(k_2)\mathcal{M}(k_3)\times B_\Phi(k_1,k_2,k_3)$. Furthermore, $F_2$ corresponds to the second-order kernel of standard perturbation theory, and $b_1^{(g_i)}$ and $b_2^{(g_i)}$ denote the linear and non-linear bias parameters for the $g_i$th tracer object, respectively. We note that when deriving the bispectrum shown above we have considered the perturbative expansion up to the tree-level order. Here, we simply neglect the higher-order loop contributions because they are expected to be not so significant at large scales [9].

The observed power spectra and bispectra from redshift surveys are distorted by the radial motion of galaxies. In order to consider the RSD, we assume that the higher-order contributions are neglected. Then, the leading-order expression for the galaxy power-/bispectrum with the redshift-space distortion is given by [26]

$$P_s^{(g_1g_2)} = Z_1^{(g_1)}(\boldsymbol{k})Z_1^{(g_2)}(\boldsymbol{k})P_{\rm L}(k), \quad (5)$$

$$B_{{\rm grav},s}^{(g_1g_2g_3)} = \frac{1}{6}[2Z_1^{(g_1)}(\boldsymbol{k}_1)Z_1^{(g_2)}(\boldsymbol{k}_2)Z_2^{(g_3)}(\boldsymbol{k}_1,\boldsymbol{k}_2) + (g_i\text{perm})]P_{\rm L}(k_1)P_{\rm L}(k_2) + (k_i\text{perm}), \quad (6)$$

$$B_{{\rm bis},s}^{(g_1g_2g_3)} = Z_1^{(g_1)}(\boldsymbol{k}_1)Z_1^{(g_2)}(\boldsymbol{k}_2)Z_1^{(g_3)}(\boldsymbol{k}_3)B_{\rm L}(k_1,k_2,k_3), \quad (7)$$

where the linear- and second-perturbation theory kernels $Z_n^{(g)}$ are defined as

$$Z_1^{(g)}(\boldsymbol{k}) = b_1^{(g)} + f\mu^2, \quad (8)$$

$$Z_2^{(g)}(\boldsymbol{k}_1,\boldsymbol{k}_2) = \frac{1}{2}b_2^{(g)} + b_1^{(g)}F_2(\boldsymbol{k}_1,\boldsymbol{k}_2), \quad (9)$$

with $\mu$ being the cosine of the angle to the line of sight. We have dropped the contributions from the second-order velocity kernel and velocity dispersion. Since the distorted spectra are rather complicated, we instead deal only with a spherically averaged power spectrum and bispectrum in the subsequent analysis, following Refs. [8,26,27]. To do so, we first derive the monopole contributions from RSD generalized to multiple tracers. By averaging over the angle between $\boldsymbol{k}_1$ and $\boldsymbol{k}_2$ and dropping the angle-dependent term, we find the averaged power spectra and bispectra in redshift space are, respectively, given as

$$P_0^{(g_1g_2)} = a_{0,\rm pow}^{(g_1g_2)}P^{(g_1g_2)}, \quad (10)$$

$$B_{{\rm grav},0}^{(g_1g_2g_3)} = \frac{1}{6}[a_{0,\rm bis}^{(g_1g_2)}b_1^{(g_1)}b_1^{(g_2)}(b_2^{(g_3)}+2b_1^{(g_3)}F_2(\boldsymbol{k}_1,\boldsymbol{k}_2)) + (g_i\text{perm})]P_{\rm L}(k_1)P_{\rm L}(k_2) + (k_i\text{perm}), \quad (11)$$

$$B_{{\rm bis},0}^{(g_1g_2g_3)} = \frac{1}{6}(a_{0,\rm bis}^{(g_1g_2)} + (g_i\text{perm}))B^{(g_1g_2g_3)}, \quad (12)$$

where the monopole redshift-space correction are

$$a_{0,\rm pow}^{(g_1g_2)} = 1 + \frac{1}{3}(\beta^{(g_1)}+\beta^{(g_2)}) + \frac{1}{5}\beta^{(g_1)}\beta^{(g_2)}, \quad (13)$$

$$a_{0,\rm bis}^{(g_1g_2)} = \left(1+\frac{1}{3}\beta^{(g_1)}\right)\left(1+\frac{1}{3}\beta^{(g_2)}\right), \quad (14)$$

with $\beta^{(g_i)} \coloneqq f/b_1^{(g_i)}$. The function $f$ is the linear growth rate, which is defined by the logarithmic derivative of the linear density field with respect to the logarithmic of the scale factor. The above expressions are the multitracer generalization of the formula for the single tracer, given in Refs. [8,26,27].

The galaxy bias parameters can be calculated from the dark matter halo bias, if we assume that galaxies are formed in dark matter halos. To evaluate the galaxy biases, we shall use the halo bias parameters $b_\ell^{\rm h}(M,z)$ given in Ref. [28], the Sheth-Tormen mass function $\mathrm{d}n/\mathrm{d}M$ [29], and the mean number of galaxies per halo of a given mass $M$, namely the halo occupation distributions $\langle N\rangle_M$ [30] with fitting parameters given in Ref. [31]. The explicit forms of the linear and non-linear halo bias parameters $b_1^{\rm h}$ and $b_2^{\rm h}$ are given by

$$b_1^{\rm h}(M,z) = 1+\epsilon_1+E_1, \tag{15}$$

$$b_2^{\rm h}(M,z) = \frac{8}{21}(\epsilon_1+E_1)+\epsilon_2+E_2, \tag{16}$$

where

$$\epsilon_1 = \frac{q\nu^2-1}{\delta_{\rm c}}, \qquad \epsilon_2 = \frac{q\nu^2}{\delta_{\rm c}}\frac{q\nu^2-3}{\delta_{\rm c}}, \tag{17}$$

$$E_1 = \frac{2p/\delta_{\rm c}}{1+(q\nu^2)^p}, \qquad \frac{E_2}{E_1} = \frac{1+2p}{\delta_{\rm c}}+2\epsilon_1, \tag{18}$$

with $\nu=\delta_{\rm c}/\sigma(M,z)$, $\delta_{\rm c}=1.686$, $p=0.3$, and $q=0.707$. Moreover, we split whole galaxy samples into some mass-divided subsamples for each redshift bin to apply the multitracer technique. The averaged number density of galaxies for the $g_i$th mass bin, $M_{(g_i)}<M<M_{(g_{i+1})}$, is given by

$$n_{(g_i)} = \int_{M_{\rm min}} \mathrm{d}M \frac{\mathrm{d}n}{\mathrm{d}M} S_{(g_i)} \langle N\rangle_M, \tag{19}$$

where $S_{(g_i)}$ and $M_{\rm min}$ represent the selection function and the minimum mass above which we find a central galaxy in the halo, respectively. In this paper, we will simply take the top-hat form of the selection function as $S_{(g_i)} = \Theta(M-M_{(g_i)})\Theta(M_{(g_{i+1})}-M)$. We find $M_{\rm min}$ from the total galaxy number density

$$n_{\rm g} = \int_{M_{\rm min}} \mathrm{d}M \frac{\mathrm{d}n}{\mathrm{d}M} \langle N\rangle_M, \tag{20}$$

for a given $n_{\rm g}$. With these, we calculate the galaxy bias parameters for the $g_i$th mass bin from the large-scale expression

$$b_\ell^{(g_i)} = \frac{1}{n_{(g_i)}} \int_{M_{\rm min}} \mathrm{d}M \frac{\mathrm{d}n}{\mathrm{d}M} S_{(g_i)} b_\ell^{\rm h} \langle N\rangle_M (\ell=1,2). \tag{21}$$

## III. FISHER ANALYSIS

Before going into the detailed evaluation of the Fisher matrix, we shall discuss the analytic understanding of the merit of the multitracer technique in the galaxy bispectrum. Just for simplicity, first, we focus only on the galaxy power spectra and bispectra from a single mode with wavelength $k$. Moreover, we drop the contributions of the galaxy bispectrum of general triangle configurations except for the equilateral one and the effect of RSD. Then, the Fisher matrix for a given wavelength $k$ is defined as

$$\tilde{F}_{\alpha\beta}(k) = \frac{\partial \boldsymbol{B}^{\rm eq}}{\partial\theta^\alpha}\cdot[\tilde{\mathrm{C}}^{-1}(\boldsymbol{B}^{\rm eq},\boldsymbol{B}^{\rm eq})]\cdot\frac{\partial \boldsymbol{B}^{\rm eq}}{\partial\theta^\beta}, \tag{22}$$

where $\boldsymbol{B}^{\rm eq}\equiv\{B^I(k,k,k)\}$, $I$ runs over the combination of the mass bins, and $\theta^\alpha$ are free parameters. Since we are interested only in the asymptotic behavior of the Fisher matrix, the covariance matrix we consider here is assumed to be

$$\tilde{\mathrm{C}}_{IJ} = \frac{1}{6}(\hat{P}^{(g_1g_1')}\hat{P}^{(g_2g_2')}\hat{P}^{(g_3g_3')}+(\mathrm{perm})), \tag{23}$$

with $\hat{P}^{(g_ig_j')} \equiv P^{(g_ig_j')}+n_{(g_i)}^{-1}\delta^{\rm K}_{g_ig_j'}$ denoting the galaxy power spectrum including the shot-noise contamination. Here, $\delta^{\rm K}$ is a Kronecker delta function. Note that the equilateral limit of the galaxy bispectrum can be reduced to the simple form

$$B^{(g_1g_2g_3)}(k,k,k) = (b_1^{(g_1)}b_1^{(g_2)}\tilde{b}_2^{(g_3)}+(g_i\mathrm{perm}))P_{\rm L}^2(k), \tag{24}$$

where we have introduced the effective non-linear bias parameter including the contribution from PNG, which is defined as $\tilde{b}_2^{(g)} \coloneqq (b_2^{(g)}+\frac{4}{7}b_1^{(g)})+b_1^{(g)}f_{\rm NL}/\mathcal{M}$. We then perform the Fisher analysis to forecast the future constraint on the non-linearity parameter $f_{\rm NL}$. Since the explicit form of the constraint on $f_{\rm NL}$ is rather complicated, we will instead evaluate the error on the relative effective non-linear bias parameter. Let us assume two tracers of underlying dark matter density field, that is, $g_i=1,2$. In this case, $I$ runs over four bins, namely $I=\{(111),(112),(122),(222)\}$. Introducing the relative linear and non-linear bias parameters $\alpha\equiv b_1^{(1)}/b_1^{(2)}$ and $\gamma\equiv\tilde{b}_2^{(1)}/\tilde{b}_2^{(2)}$, we can rewrite the galaxy bispectrum as $B^{(222)}=:\mathcal{B}$, $B^{(111)}=\alpha^2\gamma\mathcal{B}$, $B^{(112)}=(\alpha^2+2\alpha\gamma)\mathcal{B}/3$, and $B^{(122)}=(2\alpha+\gamma)\mathcal{B}/3$. Furthermore, the covariance matrix elements are also written in terms of the relative linear bias $\alpha$ and the stochasticity parameter $r$ as $\hat{P}^{(22)}=\mathcal{P}(1+X_2)$, $\hat{P}^{(11)}=\mathcal{P}(\alpha^2+X_1)$, and $\hat{P}^{(12)}=r\alpha\mathcal{P}$ with $X_{g_i}=1/(n_{(g_i)}\mathcal{P})$. Assuming little stochasticity $(r\to1)$ and

computing the error on the parameter $\gamma$ in the small shot-noise limit ($X_{g_i} \to 0$), we obtain the leading-order term of the unmarginalized $1\sigma$ error on the parameter $\gamma$ in the noise/power ratio for both tracers:

$$\tilde{\sigma}^2(\gamma) \equiv \tilde{F}^{-1}_{\gamma\gamma} \approx \frac{3\mathcal{P}^3}{\mathcal{B}^2}\{X_1 + \alpha^2 X_2 + \alpha^2(1-r^2)\}. \quad (25)$$

This implies that the error on the relative effective non-linear bias $\gamma$ from a single mode can be much less than unity if there is little stochasticity and the field is oversampled. Therefore, it is expected that with the multitracer technique we could measure PNG via the galaxy bispectrum without the CV noise, even if the type of PNG is nonlocal such as the equilateral and orthogonal types.

Let us numerically investigate the expected constraint on the non-linearity parameters with the multitracer technique, based on the full Fisher analysis. In order to evaluate the expected future constraints, we calculate the Fisher matrix for the bispectrum, which is obtained by summing over all possible triangular configurations. The explicit expression is given by [32]

$$F_{\alpha\beta} = \sum_{k_1,k_2,k_3=k_{\rm min}}^{k_{\rm max}} \frac{\partial \boldsymbol{B}}{\partial\theta^\alpha}\cdot[{\rm C}^{-1}(\boldsymbol{B},\boldsymbol{B})]\cdot\frac{\partial \boldsymbol{B}}{\partial\theta^\beta}, \quad (26)$$

where $\boldsymbol{B} = \{B_0^I(\boldsymbol{k}_1,\boldsymbol{k}_2,\boldsymbol{k}_3)\}$, $I$ runs over the mass bins $(g_1g_2g_3)$, and $\theta^\alpha$ are free parameters to be determined by observations. The marginalized expected $1\sigma$ error on parameter $\theta^\alpha$ from the Fisher matrix (26) is estimated to be $\sigma(\theta^\alpha) = \sqrt{(F^{-1})_{\alpha\alpha}}$. Assuming the Gaussian error covariance, we obtain the covariance matrix for multiple tracers as [8,27,32]

$$\begin{aligned}{\rm C}_{IJ} = &\frac{s_{\rm B}V_{\rm survey}}{36N_{\rm t}} \\ &\times[\hat{P}_0^{(g_1g_1')}(k_1)\hat{P}_0^{(g_2g_2')}(k_2)\hat{P}_0^{(g_3g_3')}(k_3) + ({\rm perm})], \quad (27)\end{aligned}$$

where $s_{\rm B}$ is the symmetric factor describing the number of a given bispectrum triangle ($s_{\rm B} = 6$, 2, and 1 for equilateral, isosceles, and general triangles, respectively) and the quantity $N_{\rm t} = V_{\rm B}/k_{\rm F}^6$ denotes the total number of available triangles with $k_{\rm F} = 2\pi/V_{\rm survey}^{1/3}$ and $V_B = 8\pi^2 k_1k_2k_3(\Delta k)^3$ being the fundamental frequency and the volume of the fundamental cell in Fourier space, respectively. Here, $\hat{P}_0^{(g_1g_2)}$ is the averaged redshift-space galaxy power spectrum including the shot-noise contamination given by $\hat{P}_0^{(g_ig_j')}(k) = P_0^{(g_ig_j')}(k) + n_{(g_i)}^{-1}\delta^{\rm K}_{g_ig_j'}$. In subsequent analysis, we assume that both the frequency gap and the minimum wavelength coincide with the fundamental frequency, namely $k_{\rm F} = \Delta k = k_{\rm min}$. Moreover, for the maximal wavelength, we choose $k_{\rm max} = \pi/(2R_{\rm min})$ with $R_{\rm min}$ such that $\sigma(R_{\rm min}, z) = 0.5$ [8]. For instance, $k_{\rm max} = 0.19[h\ {\rm Mpc}^{-1}]$ at $z = 1$, and $k_{\rm max} = 0.35[h\ {\rm Mpc}^{-1}]$ at $z = 2$. Throughout this paper, for our fiducial model, we assume a ΛCDM cosmological model with parameters $\Omega_{\rm m,0} = 0.318$, $\Omega_{\rm b,0} = 0.0495$, $\Omega_{\Lambda,0} = 0.6817$, $w = -1$, $h = 0.67$, $n_{\rm s} = 0.9619$, $k_0 = 0.05\ {\rm Mpc}^{-1}$, and $\sigma_8 = 0.835$.

Let us consider two and three mass bins such that each mass bin has the same galaxy number density, simply because the tightest constraint for $f_{\rm NL}$ is expected to be obtained when the shot-noise contributions from all mass bins become comparable. In the case of the two (three) mass bins, we have the five (seven) parameters in the Fisher matrix analysis: the four (six) bias parameters and non-linearity parameter $f_{\rm NL}$. The bias parameters are fully marginalized over when deriving the constraint on $f_{\rm NL}$. When forecasting each non-linearity parameter, we neglect the other parameters. The fiducial values of the non-linearity parameters are set to zero, and the fiducial values of the linear and non-linear bias parameters are calculated for each redshift.

To see the impact of the multitracer technique in the measurement of the galaxy bispectrum, we show the expected marginalized $1\sigma$ statistical errors on the non-linearity parameters in Figs. 1 and 2, marginalizing over the bias parameters. The fiducial survey parameters are given by the survey volume $V_{\rm survey} = 10h^3\ {\rm Mpc}^{-3}$ and the redshifts $z = 1$ and $z = 2$. When we consider the single tracer, $\sigma(f_{\rm NL})$ decreases rapidly as $n_{\rm g}$ increases and approaches the CV plateau in the large galaxy number density limit. Once the galaxy number density is high enough to reach the plateau, the further improvement in the galaxy number density does not significantly improve constraints on $f_{\rm NL}$. Even in the case of the two tracers, the plateau appears near $n_{\rm g} \approx 10^{-3}h^3\ {\rm Mpc}^{-3}$, presumably because in this region the galaxy number density is high enough to be CV limited but not enough that the CV cancellation is effective. Pushing to a higher galaxy number density, we found that the reduction of the CV noise becomes effective, and we

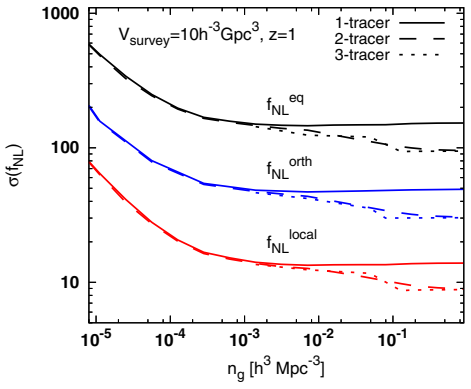


FIG. 1. $1\sigma$ marginalized errors as a function of the comoving galaxy number density, $f_{\rm NL}^{\rm eq}$ (top), $f_{\rm NL}^{\rm orth}$ (middle), and $f_{\rm NL}^{\rm local}$ (bottom) for a survey with $V_{\rm survey} = 10h^{-3}\ {\rm Gpc}^3$ and $z = 1$.

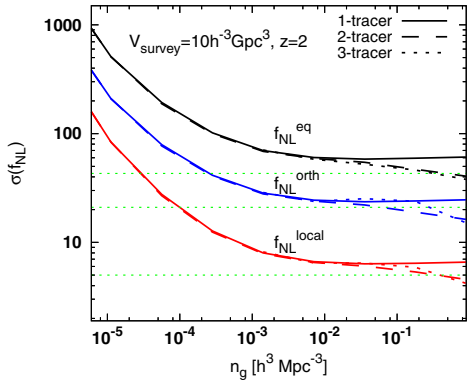


FIG. 2. Same as Fig. 1 but for $z = 2$. The green dotted lines represent the current limit from Planck [3,4].

obtain the stronger constraint on $f_{\rm NL}$. In our specific survey, the multitracer technique has the potential to constrain PNG to an accuracy of a factor of 1.4 better than the single-tracer constraints. In addition, we found that the further increase in the number of tracers leads to slight improvements of the constraints. Hence, in the subsequent analysis, we consider only the case of two mass bins.

Based on the derived analysis tool, we then apply our Fisher matrix analysis to future redshift surveys, in which we will find a large number of galaxies enough that the multitracer technique is effective. For future representative surveys, we consider the galaxy surveys conducted by Euclid and SKA Phase-2. We adopt the predicted number density of galaxies as a function of redshift, given in Table 3 of Ref. [33] for Euclid and in Table 1 of Ref. [34] for the SKA. In Fig. 3, we plot the $1\sigma$ expected marginalized contours in the $(f_{\rm NL}, b_1^{(1)})$ plane. As for $f_{\rm NL}^{\rm eq}$, the SKA can reach $\sigma(f_{\rm NL}^{\rm eq}) = 25.1$ (one tracer), 23.0 (two tracers), which is an improvement by a factor 2 compared with the Planck constraint. The constraint, from Euclid, $\sigma(f_{\rm NL}^{\rm eq}) = 30.4$ (one tracer), 30.0 (two tracers), is relatively weaker than the SKA one. The constraints on $f_{\rm NL}^{\rm orth}$ from Euclid and the SKA are $\sigma(f_{\rm NL}^{\rm orth}) = 13.6$ (Euclid, one tracer), 13.1 (Euclid, two tracers), 12.4 (SKA, one tracer) and 10.2 (SKA, two tracers). The SKA is found to be more advantageous in applying the multitracer technique, simply because the low-$z$ source density provided by the SKA is

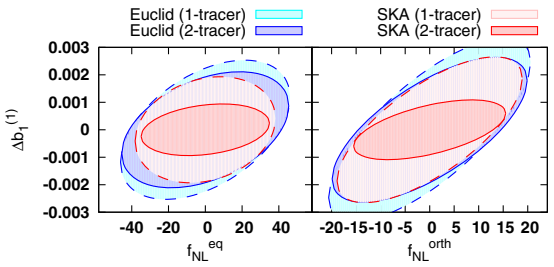


FIG. 3. Forecast $1\sigma$ marginalized contours in the $(f_{\rm NL}^{\rm eq}, b_1^{(1)})$ (left) and $(f_{\rm NL}^{\rm orth}, b_1^{(1)})$ (right) planes.

higher than the Euclid one. Therefore, we conclude that the precise measurement of the galaxy bispectrum by future galaxy surveys can probe the nonlocal-type PNG to the level comparable to or more severe than the CMB constraints.

## IV. SUMMARY

To summarize, we have discussed the potential power of the multitracer technique for the galaxy bispectrum as a possible probe of the various types of PNG. To apply the multitracer technique, we first derived the formulas for the monopole mode of RSD for the galaxy bispectrum generalized to multiple tracers. Performing the Fisher matrix analysis based on the derived formulas, we showed that the precise measurement of the galaxy bispectrum with the multitracer technique provides a powerful probe of not only the local but also nonlocal types of PNG without the CV noise. Particularly, in the region in which the galaxy number density is high enough, even for the case of two tracers, the reduction of the CV noise due to the effect of the multiple tracers becomes effective, and we obtain the stronger constraints on parameters than the single-tracer constraints. Based on these facts, we also found that the planned galaxy surveys in the next decade indeed have the potential to be competitive with current and future CMB measurements.

In this paper, we have made several simplified assumptions. We have considered only the tree-level contributions to the galaxy bispectrum from the gravitational evolution and the primordial bispectrum with the Kaiser formula. The higher-order contributions may affect the details of our result, though generic features are expected to remain the same. On the other hand, future galaxy surveys will be limited by the systematic uncertainties and the CV noises rather than statistical errors because future surveys will be able to probe the huge number of samples. Hence, we should also address the systematics of future surveys in more realistic situations. To take advantage of the multitracer technique, we need to estimate the halo mass of each galaxy, which has to be inferred from available observables. The uncertainty in estimates of the halo mass for individual galaxies may become important as systematics. When we consider a future survey that covers a wide area of sky and a significant redshift depth, a number of nuisance parameters should be included to model systematic errors. We hope to come back to these issues in the near future.

## ACKNOWLEDGMENTS

This work was supported in part by Grant-in-Aid from the Ministry of Education, Culture, Sports, Science and Technology of Japan, Grants No. 24340048, No. 26610048, No. 15H05896, No. 16H05999 (K. T.), No. No. 15K17659, No. 15H05888, and No. 16H01103 (S. Y.).

[1] E. Komatsu and D. N. Spergel, Phys. Rev. D **63**, 063002 (2001).
[2] P. Creminelli, A. Nicolis, L. Senatore, M. Tegmark, and M. Zaldarriaga, J. Cosmol. Astropart. Phys. 05 (2006) 004.
[3] P. A. R. Ade *et al.* (Planck Collaboration), Astron. Astrophys. **594**, A17 (2016).
[4] P. A. R. Ade *et al.* (Planck Collaboration), Astron. Astrophys. **571**, A24 (2014).
[5] N. Dalal, O. Dore, D. Huterer, and A. Shirokov, Phys. Rev. D **77**, 123514 (2008).
[6] S. Matarrese and L. Verde, Astrophys. J. **677**, L77 (2008).
[7] T. Matsubara, Phys. Rev. D **86**, 063518 (2012).
[8] E. Sefusatti and E. Komatsu, Phys. Rev. D **76**, 083004 (2007).
[9] S. Yokoyama, T. Matsubara, and A. Taruya, Phys. Rev. D **89**, 043524 (2014).
[10] S. Mizuno and S. Yokoyama, Phys. Rev. D **91**, 123521 (2015).
[11] I. Hashimoto, A. Taruya, T. Matsubara, T. Namikawa, and S. Yokoyama, Phys. Rev. D **93**, 103537 (2016).
[12] I. Hashimoto, S. Mizuno, and S. Yokoyama, Phys. Rev. D **94**, 043532 (2016).
[13] U. Seljak, Phys. Rev. Lett. **102**, 021302 (2009).
[14] N. Hamaus, U. Seljak, and V. Desjacques, Phys. Rev. D **84**, 083509 (2011).
[15] L. D. Ferramacho, M. G. Santos, M. J. Jarvis, and S. Camera, Mon. Not. R. Astron. Soc. **442**, 2511 (2014).
[16] D. Yamauchi, K. Takahashi, and M. Oguri, Phys. Rev. D **90**, 083520 (2014).
[17] D. Yamauchi *et al.* (SKA-Japan Consortium Cosmology Science Working Group Collaboration), *Proc. Sci.*, DSU2015 (2016) 004.
[18] D. Yamauchi and K. Takahashi, Phys. Rev. D **93**, 123506 (2016).
[19] T. D. Kitching *et al.*, arXiv:1501.03978.
[20] K. Takahashi *et al.*, arXiv:1501.03859.
[21] J. Fonseca, S. Camera, M. Santos, and R. Maartens, Astrophys. J. **812**, L22 (2015).
[22] D. Alonso and P. G. Ferreira, Phys. Rev. D **92**, 063525 (2015).
[23] D. Alonso, P. Bull, P. G. Ferreira, R. Maartens, and M. Santos, Astrophys. J. **814**, 145 (2015).
[24] S. Camera, M. G. Santos, and R. Maartens, Mon. Not. R. Astron. Soc. **448**, 1035 (2015).
[25] D. J. Eisenstein and W. Hu, Astrophys. J. **496**, 605 (1998).
[26] R. Scoccimarro, H. M. P. Couchman, and J. A. Frieman, Astrophys. J. **517**, 531 (1999).
[27] E. Sefusatti, M. Crocce, S. Pueblas, and R. Scoccimarro, Phys. Rev. D **74**, 023522 (2006).
[28] R. Scoccimarro, R. K. Sheth, L. Hui, and B. Jain, Astrophys. J. **546**, 20 (2001).
[29] R. K. Sheth and G. Tormen, Mon. Not. R. Astron. Soc. **308**, 119 (1999).
[30] J. L. Tinker, D. H. Weinberg, Z. Zheng, and I. Zehavi, Astrophys. J. **631**, 41 (2005).
[31] C. Conroy, R. H. Wechsler, and A. V. Kravtsov, Astrophys. J. **647**, 201 (2006).
[32] R. Scoccimarro, E. Sefusatti, and M. Zaldarriaga, Phys. Rev. D **69**, 103513 (2004).
[33] L. Amendola *et al.*, arXiv:1606.00180.
[34] P. Bull, S. Camera, A. Raccanelli, C. Blake, P. G. Ferreira, M. G. Santos, and D. J. Schwarz, *Proc. Sci.*, AASKA14 (2015) 024.